Journal of Power Sources 244 (2013) 597–600

Contents lists available at SciVerse ScienceDirect

Journal of Power Sources

journal homepage: www.elsevier.com/locate/jpowsour

Short communication

Electrochemical performance of all-solid-state lithium batteries with Sn_4P_3 negative electrode

Ai Ueda [a], Motohiro Nagao [a], Akiko Inoue [a], Akitoshi Hayashi [a], Yoshikatsu Seino [b], Tsuyoshi Ota [b], Masahiro Tatsumisago [a,*]

[a] Department of Applied Chemistry, Graduate School of Engineering, Osaka Prefecture University, 1-1 Gakuen-cho, Naka-ku, Sakai, Osaka 599-8531, Japan
[b] Idemitsu Kosan Co., Ltd., Kami-izumi 1280, Sodegaura, Chiba 299-0293, Japan

HIGHLIGHTS

- All-solid-state cells with Sn_4P_3 active material and a sulfide electrolyte were fabricated.
- The solid-state cell exhibited the initial capacity of 1080 mA h g^{-1} and efficiency of 91%.
- Charge–discharge mechanism of Sn_4P_3 in the solid-state cell was investigated.
- The solid-state cell with the working electrode including only Sn_4P_3 operated.

ARTICLE INFO

Article history:
Received 25 September 2012
Received in revised form
14 December 2012
Accepted 14 January 2013
Available online 18 January 2013

Keywords:
All-solid-state battery
Lithium battery
Tin phosphide
Negative electrode
Sulfide solid electrolyte

ABSTRACT

All-solid-state lithium secondary batteries have been studied as new energy storage devices with safety and reliability. To enhance the energy density of the batteries, negative electrode materials with high capacity have been actively studied. Tin phosphide Sn_4P_3 has a high theoretical capacity and forms Li_3P with Li ion conductivity in the initial lithium insertion. Li_3P would act as a matrix suppressing the volume change and giving lithium ion conduction paths. In this study, Sn_4P_3 was prepared by mechanical milling and electrochemical performance of all-solid-state cells with the Sn_4P_3 was evaluated. The working electrode of all-solid-state cell consist of Sn_4P_3, solid electrolyte (SE) and acetylene black (AB) for smooth conduction of lithium ion and electron. The cell with the Sn_4P_3 composite electrode showed the first discharge capacity of 1080 mA h g^{-1} and the initial columbic efficiency of 88%. Moreover, Sn_4P_3 was applied to the working electrode without SE and AB and its cell performance was evaluated. The cell discharged and charged, and showed the first discharge capacity of 670 mA h g^{-1}. Sn_4P_3 is thus a favorable negative electrode material to improve energy density of all-solid-state cells.

1. Introduction

Rechargeable Li ion batteries are widely used as a power source for portable electronic devices, and recently have attracted much attention as a large-scale power source for electric vehicles and plug-in hybrid electric vehicles. However, batteries for large-scale power applications require much safety and reliability. All-solid-state lithium secondary batteries, using non-flammable inorganic solid electrolyte instead of organic liquid electrolyte, have been studied as new energy storage devices because of high safety and reliability [1]. To achieve higher energy density of the all-solid-state battery, negative electrode materials with high capacity are required. Carbon materials such as graphite (theoretical capacity: 372 mA h g^{-1}) are commonly used as a negative electrode material for lithium secondary batteries [2]. However, higher capacity alternatives are being actively pursued. Lithium alloys such as Li–Si and Li–Sn have high theoretical capacity (Li–Si: 4200 mA h g^{-1}, Li–Sn: 990 mA h g^{-1}), but they result in poor cyclability due to a large volume change during charge–discharge [3]. Recently, various composite materials including metal oxides, multiphase alloys, and intermetallic compounds have been studied as alternatives to the carbon material for Li ion batteries with liquid electrolyte [4–7]. These materials showed much higher capacities than carbon materials and improved the cycle performance relative to lithium alloy materials. The cause of enhancement of cycle performance in these Li-alloy-based materials was understood by using an inactive matrix concept [4]. Li-alloy-based materials form inactive matrix during the cycling. The inactive matrix is considered to suppress the volume change of

* Corresponding author. Tel./fax: +81 72 2549331.
E-mail address: tatsu@chem.osakafu-u.ac.jp (M. Tatsumisago).

0378-7753/$ – see front matter © 2013 Elsevier B.V. All rights reserved.
http://dx.doi.org/10.1016/j.jpowsour.2013.01.061

alloying reaction, and keeps the electrode particles mechanically connected together resulting in reversible alloying.

Among these materials, metal phosphides also have attracted attention recently for their reversibility and large amount of lithium storage at relatively low potential [8–12]. Generally, metal phosphide materials have an attractive feature in their channeled or layered structure [13] through which lithium can be easily inserted to the host materials. In addition, lithium phosphide (Li_3P), which is formed by lithium insertion to metal phosphides, shows high lithium ion conductivity [14]; Li_3P can act as a matrix stabilizer like Li_2O in tin oxide materials. The contact area between active materials and solid electrolyte is limited in all-solid-state cell, because of point contact among solid particles. Thus, phosphide materials are considered to be suitable for the negative electrodes of all-solid-state cells because self-formation of a good lithium conduction matrix is achieved in the electrode by lithium insertion process.

Tin phosphide Sn_4P_3 (theoretical capacity: 1255 mA h g^{-1}) has been reported as the negative electrode in liquid-type cell [15,16]. Sn_4P_3 showed a high capacity and its reaction mechanism was investigated. Sn_4P_3 forms Sn and Li_3P in a discharge process and Li_3P would act as a matrix suppressing the volume change during alloying reaction and keep the electrode particles mechanically connected together. Moreover, Sn has high diffusion coefficient of Li ions [17] and Li_3P has high Li ion conductivity as mentioned above. Therefore, Sn_4P_3 is expected to be attractive material for the negative electrode with high capacity of all-solid-state lithium secondary batteries.

In this study, Sn_4P_3 was synthesized by a mechanochemical technique and applied to the negative electrode of all-solid-state cell. The electrochemical performance of all-solid-state cell with Sn_4P_3 active material and Li_2S–P_2S_5 solid electrolyte [18] was evaluated. Moreover, the structure of the electrode was analyzed after discharge and charge processes in order to discuss the discharge–charge mechanism of Sn_4P_3 in all-solid-state cells. Generally, the electrode of all-solid-state cell consists of the active material, solid electrolyte (SE) and a conducting additive such as acetylene black (AB) for easy conduction of lithium ion and electron to the active material. Sn_4P_3 has high electronic conductivity and Li_3P formed by the initial lithium insertion to Sn_4P_3 has high Li ion conductivity. Thus, Sn_4P_3 is expected to work as the negative electrode without SE and AB. Thus, the cell performance was also evaluated for the electrode consisting of only Sn_4P_3 without SE and AB.

2. Experimental

The Sn_4P_3 was prepared by the following process: Sn (99.9%, Aldrich) and red P (99.9%, Kojundo chemical) powders were used as starting materials for the mechanochemical synthesis. Stoichiometric amounts of starting materials were put into a ZrO_2 vessel (45 ml) with 10 ZrO_2 balls (10 mm diameter) and reacted in a planetary ball mill apparatus (Fritsch Pulverisette 7) with a fixed rotation speed of 370 rpm for 2 h under an Ar atmosphere. X-ray diffraction (XRD; UltimaIV, Rigaku) measurements of the prepared materials were performed using Cu Kα to identify crystalline phases. The morphology of the materials was evaluated by scanning electron microscopy (SEM; Jeol, JSM-5300). Electronic conductivity of Sn_4P_3 was measured for a powder-compressed pellet with stainless-steel electrodes by AC impedance measurements. An impedance analyzer (Solartron, 1260) was used and the frequency range was from 10 Hz to 1 MHz and applied voltage was 10 mV.

The composite working electrode consisted of the prepared Sn_4P_3, $80Li_2S{\cdot}20P_2S_5$ (mol%) glass–ceramic solid electrolyte (SE) and acetylene black (AB; Denki Kagaku Kogyo) in a weight ratio of 40:60:6. The composite working electrode was prepared by hand mixing. The active material loading of the composite electrode was 38 wt% of electrode. The working electrode with only Sn_4P_3 (without SE and AB) was also used in this study. The amount of those working electrodes was 15 mg. The $80Li_2S{\cdot}20P_2S_5$ glass–ceramic was prepared by a mechanochemical reaction process of Li_2S (Idemitsu Kosan Co., >99.9%) and P_2S_5 (Aldrich, 99%) as starting materials, with subsequent heat treatment at 210 °C for 1 h [18]. The $80Li_2S{\cdot}20P_2S_5$ glass–ceramic solid electrolyte exhibited favorable features for all-solid-state lithium cells such as high room temperature conductivity of over 10^{-3} S cm^{-1}, wide electrochemical window of over 10 V and high stability in contact with Li or Li–In alloy [19].

The electrochemical properties of Sn_4P_3 electrodes were investigated using an all-solid-state cell. The cell was fabricated using the Sn_4P_3 electrode as a working electrode, the SE and a Li–In alloy as a counter electrode. The working electrode and SE were placed in a polycarbonate tube (10 mm diameter) and pressed together under 360 MPa. Li–In alloy was placed on the surface of the solid electrolyte side of the bilayer pellet and a pressure of 120 MPa was then applied to the three-layered pellet. The three-layered pellet was finally sandwiched using two stainless-steel rods as a current collector. All the cell preparation processes were carried out in a dry Ar-filled glove box. Electrochemical tests were conducted at several constant current densities from 0.064 to 3.2 mA cm^{-2} at room temperature under an Ar atmosphere using a charge–discharge measurement device (BTS-2004, Nagano Co.). The voltage range of charge–discharge was −0.6 V to 1.9 V vs. Li–In.

3. Results and discussion

The XRD patterns of the mixture of Sn and red P and the sample synthesized by mechanical milling for the mixture are shown in Fig. 1. Red P has amorphous structure, and thus all peaks of the mixture are attributable to Sn (JCPDS#072-3240). All peaks of the sample synthesized by mechanical milling are attributable to Sn_4P_3 (JCPDS#071-2221), indicating that Sn_4P_3 was prepared by mechanical milling.

Fig. 2 shows the scanning electron microscope (SEM) image of the prepared Sn_4P_3 powders. The Sn_4P_3 consists of agglomerated

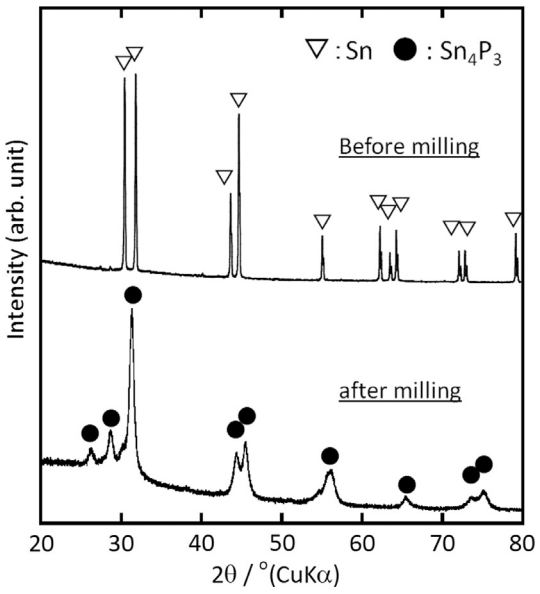

Fig. 1. XRD pattern of Sn_4P_3 prepared by mechanical milling.

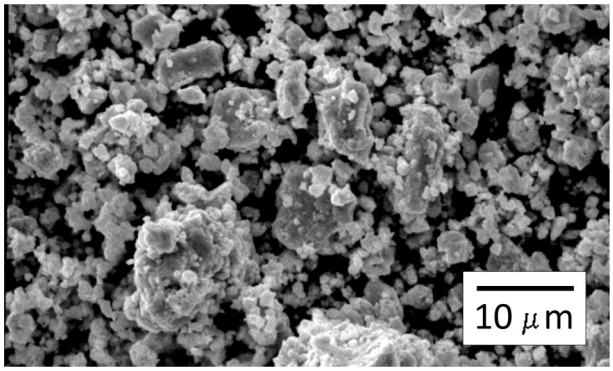

Fig. 2. SEM image of Sn_4P_3 particles.

particles of about 1–10 μm in size. The prepared Sn_4P_3 showed the electronic conductivity of 0.83 S cm^{-1} at 25 °C.

Fig. 3 shows the discharge–charge curves of the all-solid-state cell with Sn_4P_3 negative electrode at 0.064 mA cm^{-2}. The composite electrode with Sn_4P_3, SE and AB was used as a working electrode. The Li–In alloy was used as a counter electrode, because Li–In alloy exhibits a stable voltage plateau at 0.62 V vs. Li^+/Li in an all-solid-state cell with a sulfide solid electrolyte [20]. The right side ordinate axis in Fig. 3 represents the electrode potential vs. Li^+/Li, which was calculated on the basis of the potential difference between the Li–In and Li electrodes (0.62 V). The obtained capacity was normalized by the weight of Sn_4P_3 in the electrode. In this study, "discharge" is defined as lithium insertion process to Sn_4P_3.

The potential profiles of all-solid-state cell with Sn_4P_3 were similar to that of the liquid-type cell [15,16]. The discharge–charge mechanism of Sn_4P_3 reported in liquid-type cell is shown as follows:

$$Sn_4P_3 + 3Li^+ + 3e^- \rightarrow 4Sn + 3LiP \quad (1)$$

$$3LiP + 6Li^+ + 6e^- \rightarrow 3Li_3P \quad (2)$$

$$4Sn + 4xLi^+ + 4xe^- \rightarrow 4Li_xSn \quad (0 \le x \le 4.4) \quad (3)$$

Some plateaus were observed in discharge process; the first and second plateaus centered at ca. 0.9 V and 0.6 V vs. Li^+/Li are considered to be the conversion reactions of (1) and (2), respectively. Theoretical capacity of the conversion reactions is calculated to be ca. 450 mA h g^{-1}. The third plateau centered at ca. 0.35 V vs. Li^+/Li

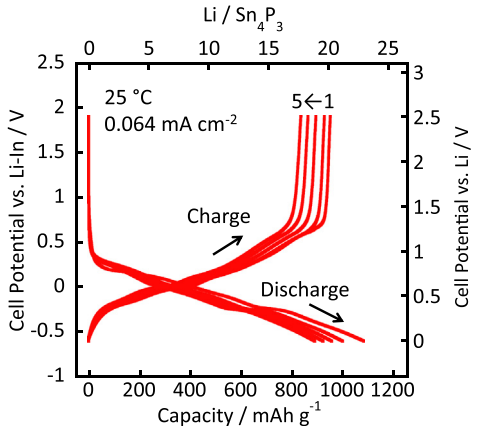

Fig. 3. Discharge–charge curves of the all-solid-state cell with the Sn_4P_3 composite as a working electrode at 0.064 mA cm^{-2}.

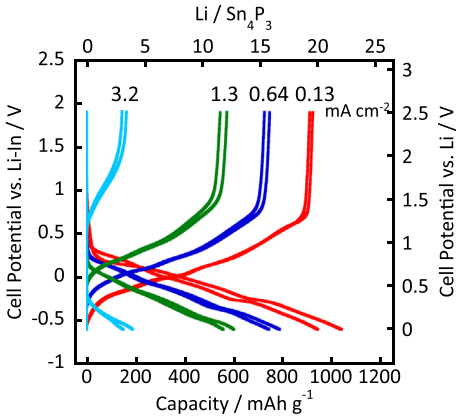

Fig. 4. Discharge–charge curves of the all-solid-state cell with the Sn_4P_3 composite as a working electrode at different current densities.

was observed and then the potential fell down to 0 V vs. Li^+/Li. In this potential range, alloying reaction of (3) proceeded.

The cell showed the first discharge and charge capacities of 1080 mA h g^{-1} and 950 mA h g^{-1}, and the first coulombic efficiency of 88% at 0.064 mA cm^{-2}. The initial coulombic efficiency of the all-solid-state cell was higher than that of the cells with a liquid electrolyte (below 80%) [15,16]. The cell kept the discharge capacity of 890 mA h g^{-1} for 5 cycles and it is calculated to be 83% of the first discharge capacity. The cycle performance of the cell will be discussed later.

Fig. 4 showed the discharge–charge curves of the Sn_4P_3 cell at 0.13, 0.64, 1.3 and 3.2 mA cm^{-2}. The cell showed the first discharge capacity of 600 mA h g^{-1} even at 1.3 mA cm^{-2}. However, the capacity largely decreased at a high rate of 3.2 mA cm^{-2} (2.6 C).

In order to discuss the reaction mechanism of Sn_4P_3 in detail, the working electrode was analyzed by XRD after the initial discharge and charge processes. The XRD patterns of the working electrode at the current collector side are shown in Fig. 5. Silicon was used as an internal standard for XRD measurements. Li_2S which remained in the SE was partially observed in the working electrodes. The diffraction peaks of Sn_4P_3 were observed before discharge–charge

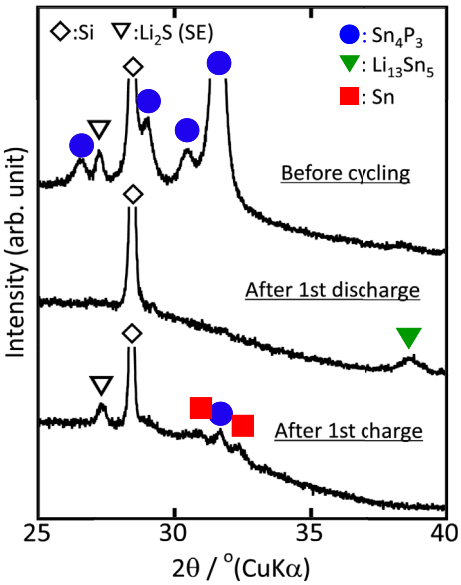

Fig. 5. XRD patterns of the Sn_4P_3 composite as a working electrode before and after the initial discharge–charge process.

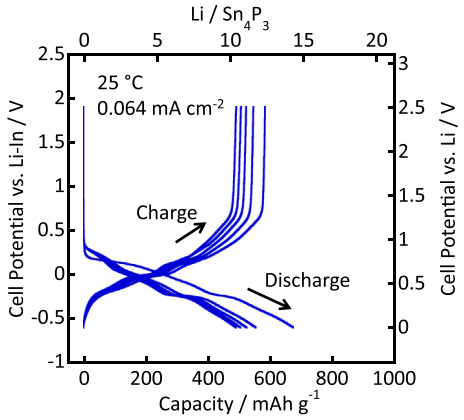

Fig. 6. Discharge–charge curves of the all-solid-state cell with only Sn_4P_3 as a working electrode at 0.064 mA cm^{-2}.

process. After the initial discharge process, the diffraction peaks of Sn_4P_3 disappeared and a broad peak attributable to $Li_{13}Sn_5$ alloy (JCPDS#071-9518) appeared. Although the formation of lithium phosphide, LiP and Li_3P, was not confirmed by XRD, Sn ions in Sn_4P_3 were reduced and metallic tin and lithium phosphide would be formed by lithium insertion, and then Li–Sn alloy was formed. The formation of Li_3P after the initial discharge was confirmed by Raman spectroscopy (the spectrum is not shown.) Further studies about the existence of lithium phosphides will be done in the near future. After the initial charge process, the diffraction peaks of $Li_{13}Sn_5$ alloy disappeared and those of Sn and Sn_4P_3 appeared. It is noted that re-formation of Sn_4P_3 was observed. In the liquid-type cell [13], the electrochemical reactions were reported to proceed in order of equations (1)–(3) as mentioned above, and the first two reactions (Sn_4P_3 to give Sn + LiP, and LiP to Li_3P) were not reversible. However, Sn_4P_3 was partially formed again in the all-solid-state cell. The re-formation of Sn_4P_3 resulted in the higher coulombic efficiency of the all-solid-state cell than that of the liquid-type cell. Further detailed analyses are needed to clarify the origin of the difference in the reaction mechanism.

In general, the electrode of all-solid-state cell consists of active material, SE and AB for ease conduction of lithium ion and electron to the active material. The results mentioned above suggest that Sn_4P_3 showed high electronic conductivity and Li_3P with Li ion conductivity formed in the initial discharge process. Thus, Sn_4P_3 itself is expected to work as a negative electrode without SE and AB. The use of only Sn_4P_3 active material leads to the improvement of energy density of the cell per weight of the working electrode. Thus, Sn_4P_3 was applied to the negative electrode without SE and AB.

The discharge–charge curve of the cell with only Sn_4P_3 is shown in Fig. 6. The cell of Sn_4P_3 was discharged and then charged without SE and AB. The potential profile of the cell without SE and AB was similar to that of the cell with SE and AB as shown in Fig. 3. The cell showed the first discharge and charge capacities of 670 mA h g^{-1} and 580 mA h g^{-1}, respectively, and the first coulombic efficiency of 86% at 0.064 mA cm^{-2}. The cell kept the discharge capacity of 487 mA h g^{-1} for 5 cycles and it is calculated to be 73% of the first discharge capacity. Although the irreversible capacity of the cell of the Sn_4P_3 electrode without SE and AB was somewhat larger than that of the cell of the Sn_4P_3 electrode with SE and AB, the first discharge capacity in terms of the total weight of the working electrode of the former cell was much larger than that of the latter cell. The use of only active material for the electrode is effective in achieving higher energy density of all-solid-state cell, and Sn_4P_3 is an appropriate negative electrode for all-solid-state cells.

4. Conclusion

Sn_4P_3 was synthesized by a mechanochemical technique. The all-solid-state cell of the Sn_4P_3 working electrode showed the first discharge capacity of 1080 mA h g^{-1} and high coulombic efficiency of 88%. From the XRD analysis of the Sn_4P_3 working electrode, Sn_4P_3 was partially formed again in the initial charge process. To achieve the large energy density of the cells, Sn_4P_3 was applied to the electrode of all-solid-state cell without SE and AB. The cell with only Sn_4P_3 was discharged and charged at room temperature. This is because that Sn_4P_3 showed high electronic conductivity and Li_3P with Li ion conductivity was formed in the initial discharge process.

References

[1] J.-M. Tarascon, M. Armand, Nature 414 (2001) 359–367.
[2] R. Fong, U. Sacken, J.R. Dahn, J. Electrochem. Soc. 137 (1990) 2009–2013.
[3] J.L. Tirado, Mater. Sci. Eng., R: Rep. 40 (2003) 103–106.
[4] Y. Idota, T. Kubota, A. Matsufuji, Y. Maekawa, T. Miyasaka, Science 276 (1996) 1395–1397.
[5] J.O. Besenhard, J. Yang, M. Winter, J. Power Sources 68 (1997) 87–90.
[6] K.D. Kepler, J.T. Vaughey, M. Thackeray, Electrochem. Solid-State Lett. 2 (1999) 307–309.
[7] H. Kim, J. Choi, H.-J. Sohn, T. Kang, J. Electrochem. Soc. 146 (1999) 4401–4405.
[8] D.C.S. Souza, V. Pralong, A.J. Jacobson, L.F. Nazar, Science 296 (2002) 2012–2015.
[9] R. Alcantara, J.L. Tirado, J.C. Jumas, L. Monconduit, J. Olivier-Fourcade, J. Power Sources 109 (2002) 308–312.
[10] V. Pralong, D.C.S. Souza, K.T. Leung, L.F. Nazar, Electrochem. Commun. 4 (2002) 516–520.
[11] D.C.C. Silva, O. Crosnier, G. Ouvrard, J. Greedan, A. Safa-Sefat, L.F. Nazar, Electrochem. Solid-State Lett. 6 (2003) A162–A165.
[12] K. Wang, J. Yang, J. Xie, B. Wang, Z. Wen, Electrochem. Commun. 5 (2003) 480–483.
[13] D.E.C. Corbridge, Phosphorus, fourth ed., Elsevier, Amsterdam, 1999, p. 71.
[14] G. Nazri, Solid State Ionics 34 (1989) 97–102.
[15] Y.U. Kim, C.K. Lee, H.J. Sohn, T. Kanga, J. Electrochem. Soc. 151 (2004) A933–A937.
[16] B. Leon, J.I. Corredor, J.L. Tirado, C. Perez-Vicentez, J. Electrochem. Soc. 153 (2006) A1829–A1834.
[17] R.A. Huggins, J. Power Sources 81 (1999) 13–19.
[18] A. Hayashi, S. Hama, T. Minami, M. Tatsumisago, Electrochem. Commun. 5 (2003) 111–114.
[19] A. Hayashi, S. Hama, F. Mizuno, K. Tadanaga, T. Minami, M. Tatsumisago, Solid State Ionics 175 (2004) 683–686.
[20] K. Takada, N. Aotani, K. Iwamoto, S. Kondo, Solid State Ionics 86 (1996) 877–882.